Supporting information

Tracing the impact of stack configuration on interface resistances in reverse electrodialysis by in-situ electrochemical impedance spectroscopy

Wenjuan Zhang(✉)[1,], Bo Han[2], Ramato Ashu Tufa[3], Chuyang Tang[4], Xunuo Liu[1], Ge Zhang[1], Jing Chang(✉)[1], Rui Zhang[1], Rong Mu[1], Caihong Liu[5], Dan Song[2], Junjing Li[6], Jun Ma[2], Yufeng Zhang[1]

1 Tianjin Key Laboratory of Aquatic Science and Technology, School of Environmental and Municipal Engineering, Tianjin Chengjian University, Tianjin 300384, China
2 State Key Laboratory of Urban Water Resource and Environment, Harbin Institute of Technology, Harbin 150090, China
3 Department of Inorganic Technology, University of Chemistry and Technology Prague, Technicka 5, 166 28, Prague 6, Czech Republic
4 Department of Civil Engineering, the University of Hong Kong, Hong Kong, China
5 Key Laboratory of Eco-environments in Three Gorges Reservoir Region (Ministry of Education), School of Urban Construction and Environmental Engineering, Chongqing University, Chongqing 400044, China
6 School of Environmental Science and Engineering, Tianjin Polytechnic University, Tianjin 300387, China

[*] Corresponding author. Tel.: +86 22 23085117; fax: +86 22 23085117.

E-mail addresses: wenjuanvivian@126.com (Wenjuan Zhang), changjinghit@163.com (Jing Chang)

1. *Properties of membranes and spacers*

1.1 Properties of membranes

Two commercial CEMs (CEM-Type I, CEM-Type II) and two AEMs (AEM-Type I and AEM-Type II) from Fujifilm manufacturing Europe B.V. (The Netherlands) were used in this study. The properties of the four ion exchange membranes are shown in Table S1.

Table S1 The properties of the ion exchange membranes used in the present study (Zhang et al., 2016a).

Membrane	Thickness (μm)	IEC (meq/g)	Swelling degree （%）	Fixed charge density (mol/L)	Zeta potential (mV)
AEM-Type I	118±2	1.41±0.01	41.4±1.0	3.4±0.1	65.6±2.0[a]
AEM-Type II	133±4	1.12±0.07	29.3±0.8	3.8±0.1	82.3±4.7
CEM-Type I	132±1	1.50±0.01	66.0±2.9	2.3±0.1	-80.9±1.9[b]
CEM-Type II	144±3	1.57±0.00	54.8±1.6	2.9±0.1	-90.4±1.1

1.2 Properties of spacers

Three types of woven spacers (Sefar, Switzerland) with similar open areas and porosities were applied to investigate the effects of intermembrane distance on RED performance. The properties of the spacers are shown in Supporting Information (Table S2.

Table S2 The properties of the spacer used in the present study.

Spacer	Thickness fabric (μm)	Material	Mesh opening (μm)	Open area (%)
07-1160/56	750	PET	1160	56
07-465/49	365	PET	465	49
07-265/53	200	PET	265	53

2. *RED setup*

A schematic view of the RED stack is shown in Fig. S1. The RED stack used in the present study consisted of cell pairs varying from 5 to 18. The stack was equipped with Fuji membranes with an active area of 0.01 m^2 (10 cm × 10 cm). The electrode material, with dimensions of 10 cm×10 cm, was made of titanium mesh coated with Ru-Ir mixed metal oxides (Magneto Special Anodes B.V., The Netherlands). Transparent silicone gaskets were used between the membrane

and electrode to avoid electrolyte leakage into the membrane pile. The electrode compartments, silicone gaskets, ion exchange membranes, and spacers were all kept together with four stainless steel bolts.

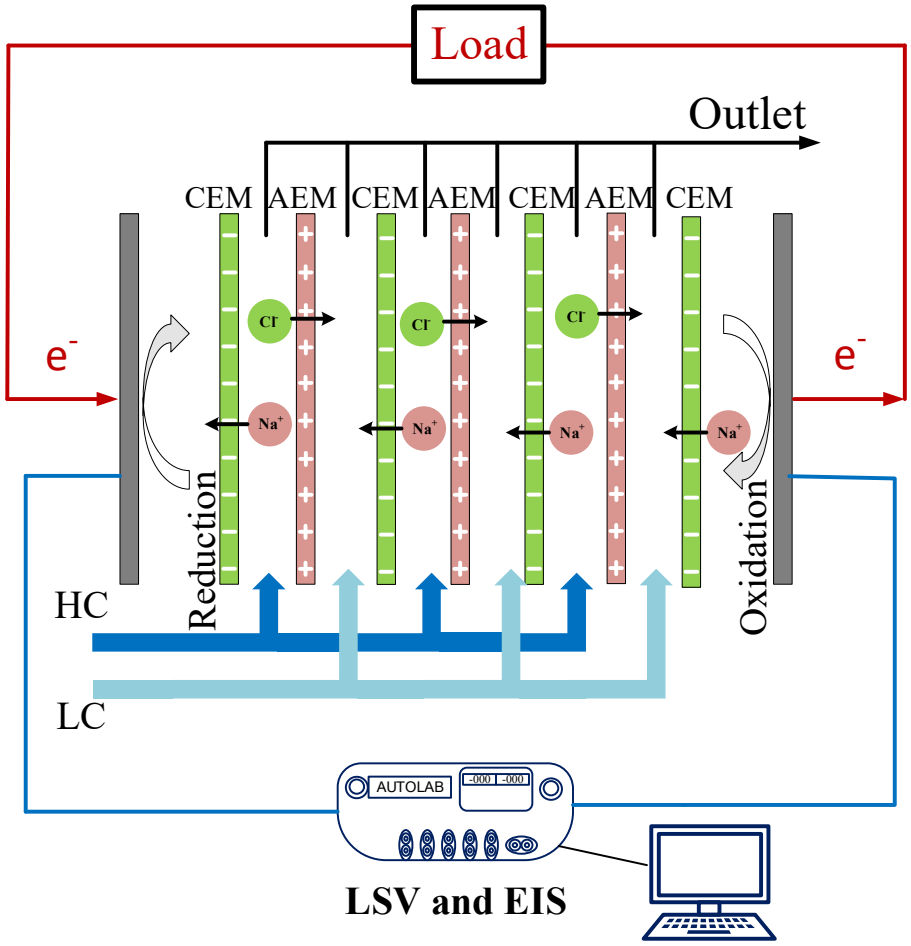

Fig. S1 Schematic illustration of the RED stack: HCC was the high concentration solution and LCC was the low concentration solution.

The equivalent circuit (Zhang et al., 2016a; Zhang et al., 2016b; Fontananova et al., 2017) used for the fitting of EIS measurements is shown in Fig. S2.

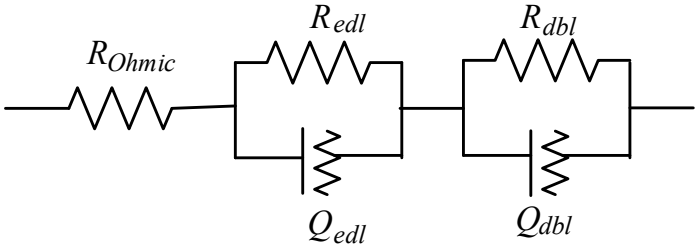

Fig. S2 Equivalent circuit (Zhang et al., 2016a; Zhang et al., 2016b; Fontananova et al., 2017) for

EIS fitting of RED stack. R_{Ohmic} represents the Ohmic resistance. R_{edl} and R_{dbl} represent the electrical double layer and the diffusion boundary layer resistance, respectively. Q_{edl} and Q_{dbl} represent the capacitance of the electrical double layer and the diffusion boundary layer, respectively.

3. Membrane transport number and permselectivity

3.1 Theoretical basis

The permselectivity of an ion exchange membrane represents the charge selectivity and the ability of a membrane to discriminate between ions with opposite charge (Długołęcki et al., 2010). There are two different methods that can be used to determine the permselectivity of ion exchange membrane: a static method and a dynamic method. In the static method, the potential gradient across an ion exchange membrane with two solutions of different concentration on both sides of membrane was measured. The apparent transport number and apparent permselectivity were calculated with the equations below.

$$\alpha_{ap} = \frac{\Delta V_m}{\Delta V_{th}} \times 100\% \quad (7)$$

$$t_{ap} = \frac{\alpha_{ap}+1}{2} \quad (8)$$

Where α_{ap} is the apparent permselectivity of ion exchange membrane (%), ΔV_m is the membrane potential measured by voltage meter (V) and ΔV_{th} is the theoretical membrane potential (V) which is calculated from the Nernst equation for a 100% pemselective membrane.

In the dynamic method, chronopotentiometry was applied in a six-compartment set-up made of plexiglass by imposing a constant current density to the system and measuring the voltage drop across the membrane as a function of time. The real transport number of ion exchange membranes can be calculated from the Sand equation below:

$$\tau = \frac{\pi D}{4}\left(\frac{C_s Z_i F}{t_m - t_s}\right)^2 \frac{1}{i^2} \quad (9)$$

Where τ (s) is the transition time that can be obtained from the chronopotentiometric curve, Z_i is the charge number of the counter-ion (Z_i=1 for Na^+ and Cl^-), C_s is the solution concentration, D is the diffusion coefficient of NaCl (1.46×10^{-9} m^2/s^4), t_m and t_s are the transport number of counter-ion in membrane and solution, respectively, and i (A) is the current density. The real permselectivity of ion exchange membrane can be obtained from the equation below

$$\alpha_{re} = 2t_m - 1 \quad (10)$$

Where α_{re} is the real permselectivity of membrane and t_m is the real transport number

The advantage of the dynamic method is that the water transport due to electro-osmosis and osmosis is taken into account.

3.2 Measurement for membrane transport number and permselectivity

The schematic view of the experimental setup used for Chronopotentiometry was shown in Fig. S3. A Metrohm Autolab potensiostat (PARSTAT302N) with two platinum electrodes and two Ag/AgCl reference electrodes was used for injecting a fixed current density and simultaneously measuring voltage drop across the membrane under investigation respectively. The solution filled in capillaries of reference electrodes was an aqueous KCl solution with a concentration of 3.5 M. Current densities above the limiting current value have to be applied to the setup to make sure the concentration at the membrane surface reach zero. CEM-Type II and AEM-Type II were used as auxiliary membranes. Before experiments, the test membranes were immersed in the solution identical to the test solution for at least 24 h. The Chronopotentiometric data of Fuji-AEM-Type II as a function of current density was shown in Fig. S4, and the Sand plot for AEM-Type II was shown in Fig. S5.

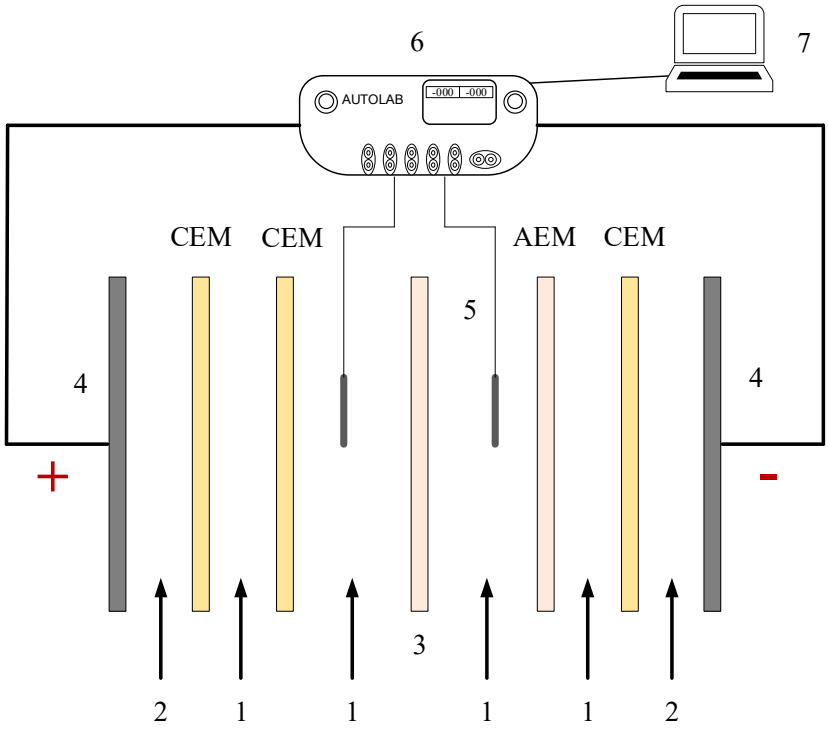

Fig. S3 Schematic view of the experimental setup used for chronopotentiometry. In this figure, 1 represents the NaCl solution (0.5 M), 2 represents the Na_2SO_4 solution (0.5 M), 3 represents the tested ion exchange membrane, 4 represents the working elctrode and counter electrode, 5 represents the referencr electrodes, 6 represents the Metrohm Autolab potensiostat, and 7 represents the computer.

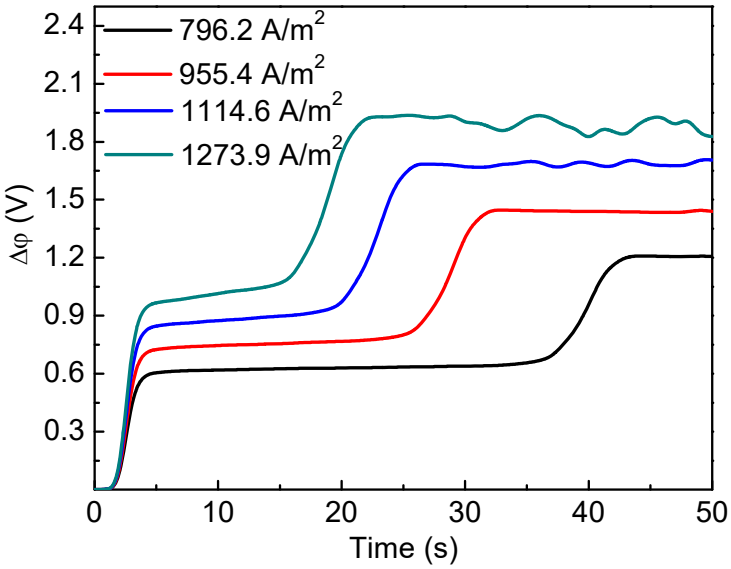

Fig. S4 Chronopotentiometric results of Fuji-AEM-Type II at different current density

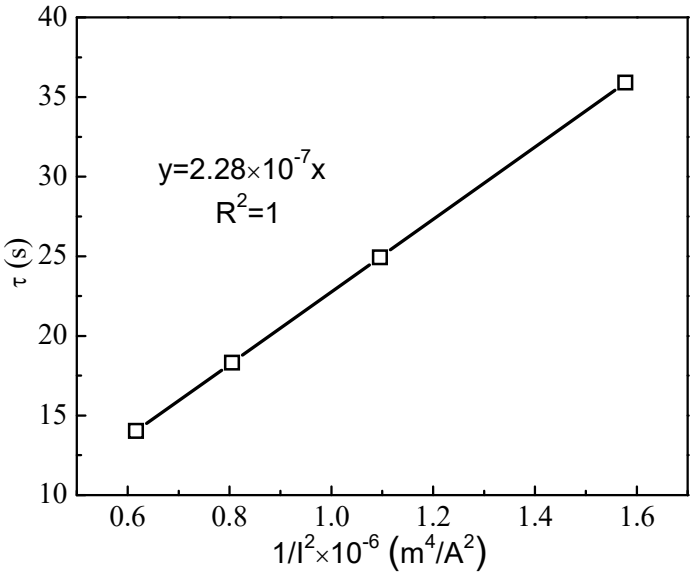

Fig. S5 Sand plot of AEM-Type II

The calculated data for transport numbers and permselectivity of ion exchange membranes from chronopotentiometry test were listed in Table S3.

Table S3 Transport numbers and permselectivity for membranes

Membrane	Transport number	Permeselectivity	Average permselectivity
AEM-Type I	0.950	0.900	0.850
CEM-Type I	0.900	0.800	
AEM-Type II	0.996	0.992	0.956
CEM-Type II	0.960	0.920	

4. RED stack resistance as a function of cell pair numbers

The experimental data for RED stack resistance as a function of cell pair numbers and the linear fitting results were shown in Fig. S6.

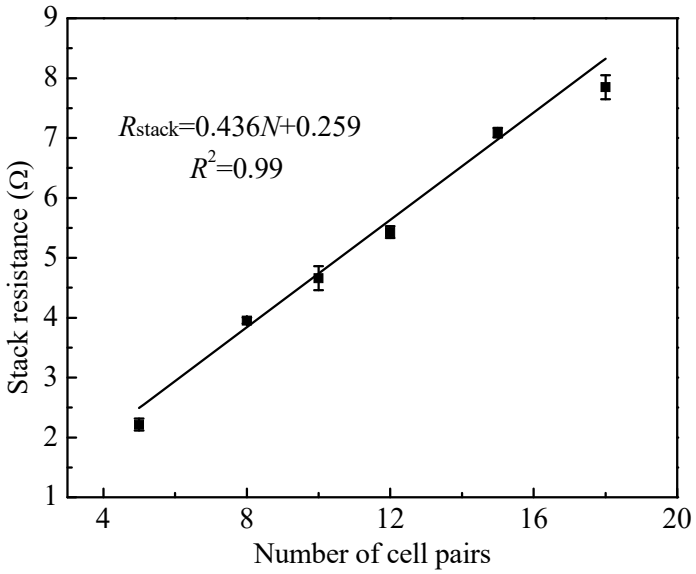

Fig. S6 The RED stack resistance as a function of cell pair numbers.

5. Experimental data and fitting data of EIS for different configurations of RED stack

EIS data and fitting data for some configurations (Table S4) of RED stack are shown in this part. Fig. S7-1a)~4a) shows the typical Nyquist plot of electrochemical impedance spectra with Z′ representing the real part and Z″ representing the imaginary part of the impedance. Fig. S7-1b)~4b) displays the corresponding Bode plot indicating the changes of phase shift and impedance module with frequency. The fitting data of RED stack according to the equivalent circuit (Fig. S2) was shown in red lines. As shown in Fig. S7, at both low frequency and high frequency, the fitting data and the experimental data showed good agreement. Indeed, the Chi-square values (χ^2) for the RED stack were in the magnitude of 10^{-5}, which indicates that the fittings (red lines) with the equivalent circuit (Fig. S2) showed good convergence. It is also proved that the EIS fitting data is well-matched with the equivalent circuit model.

Table S4 Configurations of the RED stack.

Configuration No.	Controlled parameter	Membrane	Spacer	Number of cell pairs	Flow velocity in HCC and	Flow rate of electrolyte (ml/min)

					LCC (cm/s)	
S5-1	Membrane type	Type I	PET-07-465/49	10	0.66	630
S5-2	Number of cell pairs	Type II	PET-07-465/49	5	0.66	630
S5-3				10		
S5-4	Spacer type	Type II	PET-07-1160/56	5	0.66	630

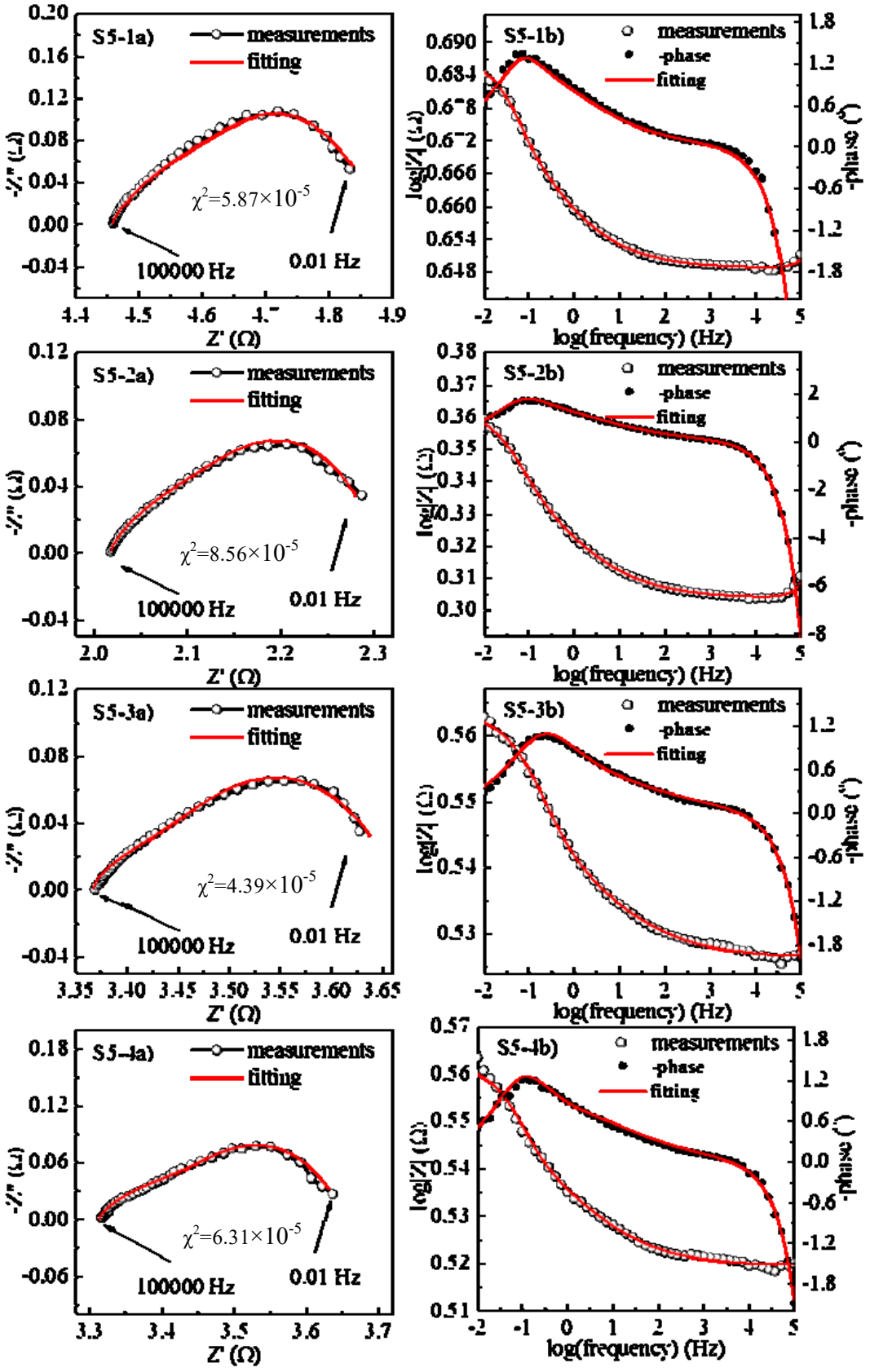

Fig. S7 Nyquist plot (a) and Bode plot (b) from EIS measurements of the RED stack with different configurations shown in table S2. Fitting curves (red lines) was the experimental data (○ and ●) fitted according to the equivalent circuit of Fig. 2.

References

Długołęcki P, Anet B, Metz S J, Nijmeijer K, Wessling M (2010). Transport limitations in ion exchange membranes at low salt concentrations. Journal of Membrane Science, 346(1): 163-171

Fontananova E, Messana D, Tufa R A, Nicotera I, Kosma V, Curcio E, Van Baak W, Drioli E, Di Profio G (2017). Effect of solution concentration and composition on the electrochemical properties of ion exchange membranes for energy conversion. Journal of Power Sources, 340: 282-293

Zhang W, Ma J, Wang P, Wang Z, Shi F, Liu H (2016a). Investigations on the interfacial capacitance and the diffusion boundary layer thickness of ion exchange membrane using electrochemical impedance spectroscopy. Journal of Membrane Science, 502: 37-47

Zhang W, Wang P, Ma J, Wang Z, Liu H (2016b). Investigations on electrochemical properties of membrane systems in ion-exchange membrane transport processes by electrochemical impedance spectroscopy and direct current measurements. Electrochimica Acta, 216: 110-119